Interference from the Second Layer in Holographic Radar

M. Inagaki[1], **T. Bechtel**[2], **and V. Razevig**[3]

[1]Walnut Ltd., 1-19-13 Saiwaicho, Tachikawa, Tokyo, Japan
[2]Department of Earth and Environment, Franklin & Marshall College, Lancaster, PA, USA
[3]Remote Sensing Laboratory, Bauman Moscow State Technical University, Russia

Abstract— Holographic radar of Rascan type produce plan view subsurface images using five simultaneous frequencies. Since it is continuous wave radar with no time-of-flight data, the reflections coming from different depths are superimposed into a single plan view. The first reflection is usually dominant on the image. However, if the reflectivity is large at the second boundary both reflected waves are received and interference occurs. As a result the image looks different from ones produced by only a first reflection. This interference might affect the proper interpretation of radar images. However, there is a benefit in that by observing the pattern of interference over five frequencies, the distance between two boundaries could be determined.

1. INTRODUCTION

Holographic radars provide a plan view as opposed to the section view provided by conventional pulsed radar An advantage of plan view is the ability to reproduce the true shape of buried objects. However, holographic radar does not allow determination of vertical structures since all the reflections from different depths at the same horizontal location are compressed onto a single horizontal plane. Any reflection event that appears on the image is actually the result of summing all the reflections from different depths. Because of attenuation, the first reflection is usually dominant. However, if the dielectric contrast is larger at a second or deeper boundary one and the distance between the first and the second reflectors is sufficiently close relative to the material attenuation, the second reflection may become strong enough to influence to the first reflection and alter the radar image. In some circumstances, this could provide data related to the separation between the two boundaries. This paper describes numerical simulations to show the interference from a second layer in selected conditions, and reproduces the theoretical predictions experimentally.

2. HOLOGRAPHIC IMAGE

Holographic subsurface radars of the Rascan type produce images based on the phase difference between the subsurface or object beam, and a reference beam produced by the surface reflection, with the recorded phase differences at different points on the scanned surface plotted as a grey scale image. Two primary causes of the observed phase difference are target depth and signal frequency. An object appears black on the radar image if the depth and frequency produce constructive interference or positive maximum, and white for negative maximum. Destructive interference or cancellation between the subsurface (object) and surface (reference) beams can also occur, leading to zero net signal for certain targets at certain frequencies. If there are two reflectors in the path of the propagating wave, reflections will occur at their two depth positions. For instance, an underground void has two boundaries; the top and the bottom of the void. In this case, the two reflections may interfere with each other, and the net amplitude of the received wave can be either strengthened or weakened depending on the separation of the reflectors for a given frequency. If the reflectivity or the first boundary is large, the effect will be comparatively small. However, if the reflectivity of the second boundary is large, the interference from the second reflection cannot be ignored (See Figure 1).

3. SIMULATION

The interference effect has been theoretically simulated using a two boundary model. The model is shown in Figure 2. In Case 1, two plastic layers are separated with a void between them. In Case 2, the bottom plastic layer is replaced by rubber. Simulations have been carried out for both cases.

Actually, reflections occur at four boundaries (top, bottom and both sides) inside the void, and there are also multiples, creating complex reflection ray paths. However, to maintain simplicity, only the basic reflections, which are obviously expected to be dominant were considered. Only the top of the void (shown as u_1 in Figure 2) and the bottom of the void (shown as u_2 in Figure 2) were included in the model as sources of spherical electromagnetic waves. Following Huygen's principle,

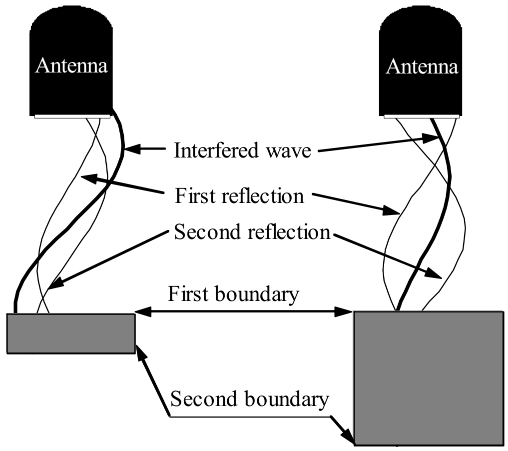

Figure 1: Interference between reflections from two boundaries.

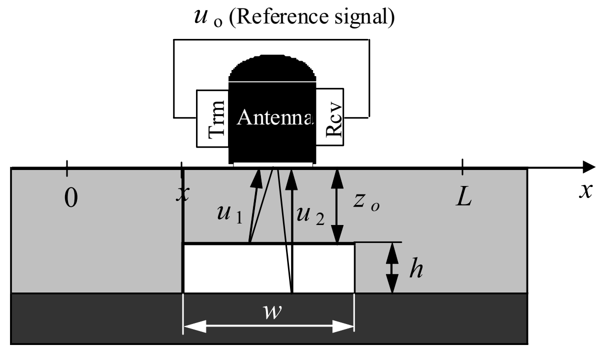

Figure 2: Model for simulation.

the response signal $u(x)$ will be the superposition of reflections from each point reflector multiplied by the roundtrip phase to that point [1]

$$u(x) = \int_0^L r(x') \left(K_1 \frac{RP^2(\theta_1)}{r_1^2} e^{i2r_1k_1} + K_2 \frac{RP^2(\theta_2)}{r_2^2} e^{i2r_2(k_1z_0+k_2h)/(z_0+h)} \right) dx', \tag{1}$$

where,

L — length of the scan line;

$r(x) = \begin{cases} 1, \ x \in [x_0, \ x_0 + w] \\ 0, \ x \notin [x_0, \ x_0 + w] \end{cases}$ — reflectivity function;

K_1, K_2 — amplitude coefficients;

RP — radiation pattern of antenna;

$r_1 = \sqrt{(x - x')^2 + z_0^2}$; $r_2 = \sqrt{(x - x')^2 + (z_0 + h)^2}$;

$k_1 = \sqrt{\varepsilon_1} 2\pi f/c$; $k_2 = \sqrt{\varepsilon_2} 2\pi f/c$ — wavenumbers;

$\theta_1 = \arccos \frac{z_0}{r_1}$; $\theta_2 = \arccos \frac{z_0+h}{r_2}$;

The term $(k_1 z_o + k_2 h)/(z_o + h)$ is included because the signal u_2 goes through the medium 1 (with wavenumber k_1) and also through the medium 2 (with wavenumber k_2).

It is necessary to know the amplitude coefficients K_1 and K_2 (note that these are different the wavenumbers denoted by the lower case letter k). When electromagnetic wave propagating in an isotropic medium with permittivity ε_1 is incident upon another isotropic medium with permittivity ε_2 (permeability μ=1 for both media), the reflection and transmission coefficients are [2]:

$$R = \left(1 - \sqrt{\varepsilon_2/\varepsilon_1}\right) / \left(1 + \sqrt{\varepsilon_2/\varepsilon_1}\right), \qquad T = 2\Big/\left(1 + \sqrt{\varepsilon_2/\varepsilon_1}\right) \tag{2}$$

In our case signal u_1 is reflected from the boundary between mediums 1 and 2. So

$$K_1 = \left(1 - \sqrt{\varepsilon_2/\varepsilon_1}\right)\Big/\left(1 + \sqrt{\varepsilon_2/\varepsilon_1}\right) \tag{3}$$

Signal u_2 goes through the boundary between media 1 and 2, then reflects at the boundary between media 2 and 3, and at last goes through the boundary between media 2 and 1. So

$$K_2 = \left(2\Big/\left(1 + \sqrt{\varepsilon_2/\varepsilon_1}\right)\right) \cdot \left(\left(1 - \sqrt{\varepsilon_3/\varepsilon_2}\right)\Big/\left(1 + \sqrt{\varepsilon_3/\varepsilon_2}\right)\right) \cdot \left(2\Big/\left(1 + \sqrt{\varepsilon_1/\varepsilon_2}\right)\right). \tag{4}$$

Using these formulae, a computer simulation has been carried out, with excerpts of the result shown in Figure 3. The reflections clearly appear at 18 mm void thickness. The reflection from the second boundary influences maximally at 33 mm void thickness for a 4.0 GHz signal frequency and at 39 mm thickness for a frequency of 3.6 GHz. The second reflector influence almost disappears at 54 mm. Two typical simulated images (non-influenced and influenced) are visually shown in Figure 4.

4. EXPERIMENT

In order to provide mutual validation, an experiment matching the simulation conditions has been carried out. The pictures of the actual model are shown in Figure 5. The upper picture is Case 1 (plastic void floor) and the bottom is Case 2 (Rubber floor). Plastic plates (thickness 3 mm each) were used for plastic layers. Rubber sheeting was for the void floor in Case 2. The nominal electrical properties of the model materials are shown in Table 1. The thickness of layer 1 is fixed at 12 mm. The void thickness is variable in 3 mm increments from 18 mm to 54 mm, and is controlled by the number of plastic plates. The experimental results are shown in Figure 6 (plastics floored void) and Figure 7 (rubber floored void).

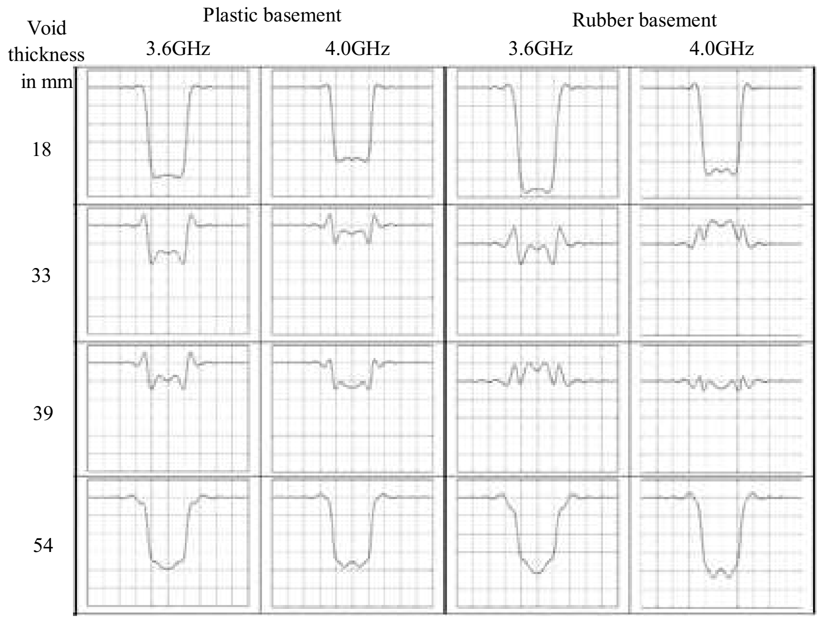

Figure 3: Simulated signal strength of superimposed reflections for two frequencies and four void thicknesses.

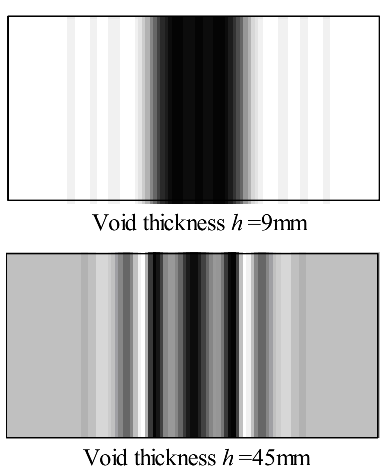

Figure 4: Simulated Rascan images for a rubber void floor with $f = 3.6$ GHz.

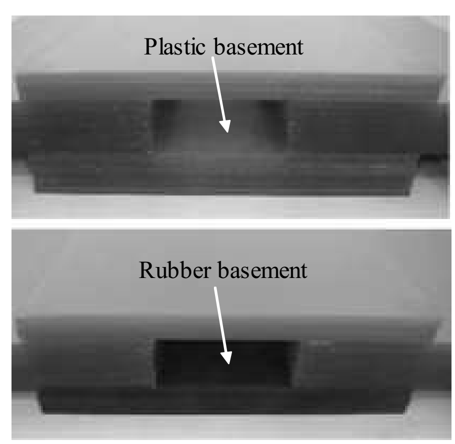

Figure 5: Specimens for experiment.

Table 1: Model electrical properties [4].

Property \ Material	Plastics	Rubber
Electric permittivity	2.7	8.3
Attenuation coefficient (1/m)	0	0.94

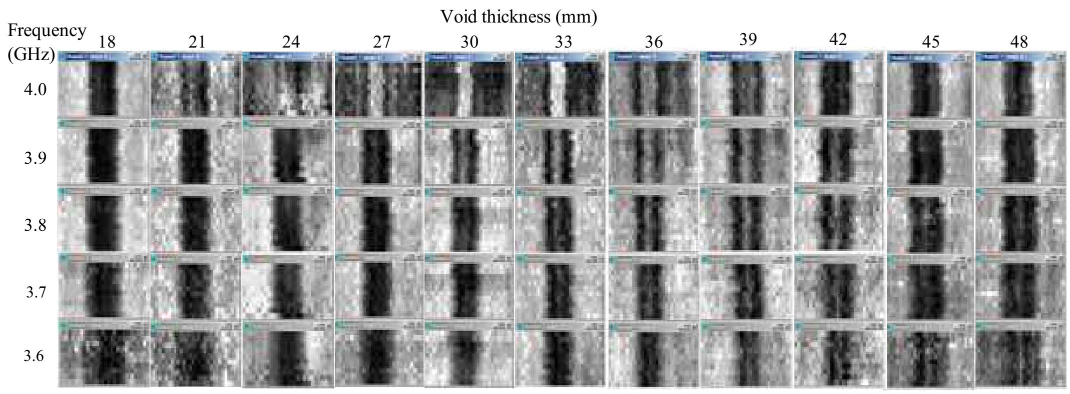

Figure 6: Actual GPR images (Plastic void floor).

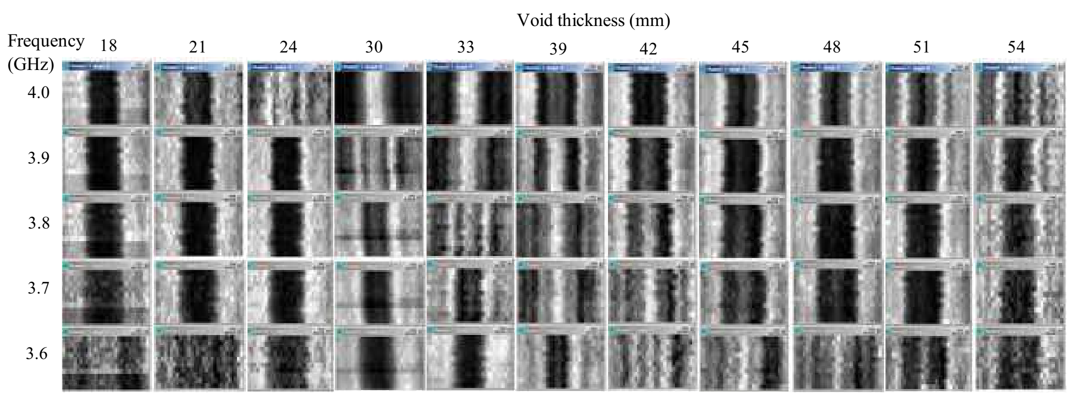

Figure 7: Actual GPR images (Rubber void floor).

The images at 18 mm void thickness appear as a black band between two grey bands. These are the typical reflected images from only the top of the void. They look very close to the simulated image (Figure 4 left). The image clearly changes with increasing void thickness. The influence becomes maximal at the 33 mm for $f = 4.0$ GHz. This is the position where the greatest interference occurs, and it is the same for the plastic and the rubber floors. The experimental phenomenon closely matches the simulation. The greatest interference shifts rightward in Figures 6 and 7 with frequency decrement, occurring at 42 mm to 45 mm for $f = 3.6$ GHz. This is particularly evident for the void with rubber floor, however, it is slightly ambiguous for the plastic floored void. The occurrence is a little shifted to thicker voids (by perhaps 3 to 5 mm) compared to the results of the simulation.

5. APPLICATION

The main advantage of holographic subsurface radar is the ability to accurately determine the plan view shape of buried objects. However the effect of target depth on the interference pattern provides depth/relief or volumetric information on the object as well. However, we have shown that the contrast pattern also depends upon the possible presence of multiple boundaries. Thus, if multiple boundaries are present, the separation and electrical property contrasts at these boundaries can affect the contrast pattern and possibly complicate the interpretation of the outline and relief or volumetric impression of the target.

There are some obvious cases where the phenomenon of interference from a second boundary could be expected. For instance, impulse radar is widely applied to underground void detection. However impulse radar detects only the location of a void and destructive testing (e.g., a boring) is needed to confirm the thickness. In roadway inspections, there are many voids detected, many of which may be very thin and do not affect the road safety. Boring is a very time-consuming work. The holographic interference phenomenon described in this paper could be used for screening whether voids are relatively thick or thin, possibly reducing the time and cost of void detection work.

6. CONCLUSIONS

Interference can occur between the reflections from the first and the second boundaries presented by targets with finite thickness for certain combinations of target thickness, boundary electrical contrasts, and signal frequency. This has been theoretically and experimentally demonstrated. This phenomenon might affect proper interpretation of holographic radar images. However, since the degree of interference is partly dictated by the distance between two reflective boundaries this phenomenon could be useful. An example is the determination of underground void thickness based on imaging using separate discrete frequencies.

REFERENCES

1. Sheen, D. M., D. L. McMakin, and T. E. Hall, "Three-dimensional millimeter-wave imaging for concealed weapon detection," *IEEE Transactions on Microwave Theory and Techniques*, Vol. 49, No. 9, September 2001.
2. Kong, J. A., *Electromagnetic Wave Theory*, Wiley-Interscience, 1975, 1986, 1990; EMW Publishing since 1998, 2000, 2005, latest Edition: 1016 pages published, May 2008.
3. Windsor, C. G., A. Bulletti, L. Capineri, P. Falorni, S. Valenini, M. Inagaki, T. D. Bechtel, E. Bechtel, A. V. Zhuravlev, and S. I. Ivashov, "Depth information from holographic radar scans," *PIERS Proceedings*, 757–761, Moscow, Russia, August 18–21, 2009.
4. Inagaki, M. and Y. Okiyasu, "Attenuation coefficients of complex materials" *Proceedings of the Ninth International Conference on Ground Penetrating Radar, GPR2008*, Birmingham, UK, June 16–19, 2008
5. Inagaki, M., C. G. Windsor, T. Bechtel, E. Bechtel, S. Ivashov, and A. Zhuravlev, "Three-dimensional views of buried objects from holographic radar imaging," *PIERS Proceedings*, Moscow, Russia, August 18–21, 2009.